J. Am. Soc. Mass Spectrom. (2018) 29:382–392
DOI: 10.1007/s13361-017-1835-4

RESEARCH ARTICLE

Collision Induced Dissociation of Benzylpyridinium-Substituted Porphyrins: Towards a Thermometer Scale for Multiply Charged Ions?

Katrina Brendle,[1] Max Kordel,[1] Erik Schneider,[1] Danny Wagner,[2,3] Stefan Bräse,[2,3] Patrick Weis,[1] Manfred M. Kappes[1,4]

[1]Institute of Physical Chemistry, Karlsruhe Institute of Technology, Kaiserstr. 12, 76131, Karlsruhe, Germany
[2]Institute of Organic Chemistry, Karlsruhe Institute of Technology, Kaiserstr. 12, 76131, Karlsruhe, Germany
[3]Institute of Toxicology and Genetics, Hermann-von-Helmholtz-Platz 1, D-76344, Eggenstein-Leopoldshafen, Germany
[4]Institute of Nanotechnology, Karlsruhe Institute of Technology, 76021, Karlsruhe, Germany

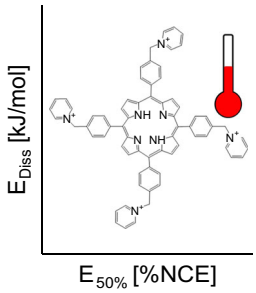

Abstract. We have determined breakdown curves for a range of multiply charged benzylpyridinium-substituted porphyrin cations by collision induced dissociation measurements (CID) as mediated by resonant pulsed radio-frequency (rf) excitation in a helium-filled linear ion trap. Measurements were compared with the predictions of DFT calculations. We find a linear correlation between experimental fragmentation thresholds (in instrumental units of "normalized collision energy") and theoretical dissociation energies, suggesting that these species can be used as calibrants to gauge the fragmentation energetics of closely related systems. We have confirmed this by also studying the fragmentation thresholds of metalloporphyrin-based ions – including multiply negatively charged metalloporphyrin oligomers. Unfortunately, the slope of the linear correlation obtained for benzylpyridinium-substituted porphyrin multications differs significantly from that obtained by us for a set of smaller, singly charged substituted benzylpyridines put forward as "thermometer" ions in previous work. Multiplying the threshold energies in an ad hoc fashion by the ion charge basically reconciles both calibration curves. We conclude that one should use caution when applying small, singly charged benzylpyridines as calibrants to gauge the CID of large, multiply charged ions in ion-trap mass spectrometers.

Keywords: Collision induced dissociation, Thermometer ions, Porphyrins, Benzyl-pyridine

Received: 9 August 2017/Revised: 8 October 2017/Accepted: 10 October 2017/Published Online: 30 October 2017

Introduction

Modern mass spectrometers often feature MS/MS capabilities. Usually, this involves collision induced dissociation (CID), a process in which mass selected parent ions are fragmented and the resulting charged fragments quantified. Such measurements yield structural and energetic information and correspondingly, CID has developed into a powerful and ubiquitous analytical tool [1]. Energy-dependent CID [2] measurements can be deconvoluted to yield breakdown curves in which the relative parent intensity (ratio of the parent ion intensity and the total ion intensity) is plotted as a function of the systematically varied excitation parameters – typically excitation energy and fragmentation time. Despite the widespread use of CID, determining bond energies from CID breakdown curves is far from straightforward [3]. Ideally, a well-thermalized ion packet is excited to a well-defined internal energy and the resulting decay is then probed for an infinitely long time (to rule out kinetic shifts). None of these conditions are usually fulfilled. First, the ion source produces ions at temperatures that differ significantly from room temperature (often higher) but which are not accurately known. Furthermore, the internal excitation level of the ions when probed also depends on the transfer ion optics to the mass spectrometer and whether or not they are thermalized prior to the CID step. As a consequence, their energy can be modified during the transfer

Electronic supplementary material The online version of this article (https://doi.org/10.1007/s13361-017-1835-4) contains supplementary material, which is available to authorized users.

Correspondence to: Patrick Weis; *e-mail:* patrick.weis@kit.edu

to the CID collision cell. Another complication affects the collisional excitation: whereas in classic triple-quadrupole instruments, all parent ions are accelerated to a well-defined kinetic energy distribution prior to the collision with a bath gas (usually at room temperature), this is typically not the case in modern ion-trap mass spectrometers. Here, the mass selected parent ion is resonantly excited for some set time period by a radio-frequency (rf) electrical field [4]. During this excitation sequence the ions undergo multiple collisions with the bath gas and may ultimately dissociate. The fragments are off-resonance, i.e., they are not further excited once formed. While the rf-amplitude and excitation time is well defined, the amount of energy transferred depends crucially on the rf-frequency in relation to the mass of the parent ion. For obvious reasons, the excitation time is limited and is typically on the time scale of milliseconds to seconds. Heavy parent ions with a large number of degrees of freedom have to be excited to internal energies significantly above the dissociation threshold in order to dissociate on this time scale – a well-known phenomenon called kinetic shift [5]. Finally, it is not clear a priori whether the detection efficacy is the same for parent and fragments, especially if the ions need to be transferred from the collision cell/ion trap to a detecting mass spectrometer. In short, CID experiments are easy to perform, but difficult to analyze quantitatively. Instead of trying to determine all relevant experimental parameters and work out the excitation energy from them, another approach is to calibrate the instrument by using "thermometer ions" with well-known fragmentation energetics.

Several substances have been introduced as molecular thermometers, such as leucine-enkephalin [6–8], tetraethylsilane ions [9, 10], transition-metal carbonyl complexes [9, 11], and substituted benzylpyridinium salts [12–32]. Among these, benzylpyridinium ions have been used most often because their fragmentation pattern is comparatively simple. The dominant decay channel comprises the loss of a neutral pyridine molecule: $[R\text{-}C_6H_4\text{-}CH_2\text{-}NC_5H_5]^+ \rightarrow [R\text{-}C_6H_4\text{-}CH_2]^+ + NC_5H_5$. The corresponding fragmentation is thought to occur through a loose transition state, i.e., it can be looked upon as a direct bond cleavage without a reverse activation barrier [13, 14, 16, 18, 19]. This greatly facilitates the theoretical modeling of the rate constants for fragmentation since the vibrational frequencies of the transition state can be interpolated by the frequencies of parent and fragments. In a very pragmatic approach using a series of differently substituted benzylpyridinium ions, Zins et al. [13] have shown that there is a strong linear correlation between the experimentally determined breakdown curve (obtained from the ratio of parent ion to total ion intensity) and the energy difference between parents and fragments as obtained from quantum chemical calculations. In their studies, which were performed using two similar ion-trap instruments (Finnigan LCQ), they did not try to calculate the internal energy of the collisionally activated parent species based on the experimental parameters. Instead, they measured the parent and fragment ion intensities as function of the instrumental energy scale, the so called "normalized collision energy", NCE [33]. This software-controlled energy scale is designed to achieve similar degrees of fragmentation at similar NCE settings, independent of the *m/z* ratio of the parent ion. As a consequence, for a given NCE value, the resonance rf amplitude that is applied increases with *m/z* – typically with a linear dependence. For each ion species, it turns out that the breakdown curve obtained (as function of NCE) can be characterized quite well by only one molecule-specific parameter. Zins et al. demonstrated in their study of the breakdown curves of 15 substituted benzylpyridinium ions that both the threshold energies, $E_{50\%}$, (the NCE value corresponding to equal parent and fragment ion intensities) and the appearance energies AE (corresponding to a linear extrapolation of the breakdown curve from $E_{50\%}$ to the fragmentation onset) correlate strongly with the calculated dissociation energies. This correlation allows a very simple calibration of the CID energy scale of the respective instrument, without also having to calculate fragmentation rate constants on the basis of RRKM [34] simulations.

By inference, other parent ions with similar $E_{50\%}$ or AE in units of NCE should also have similar fragmentation barriers. Does this in fact hold true over a wider *m/z* range (and in particular also for more highly charged species) than accessed in the above mentioned study of small, singly charged benzylpyridinium species? Here we follow up on this question by performing analogous measurements on a set of chemically related but significantly larger thermometer ions using an ion-trap based instrument (Thermo LTQ-XL Orbitrap) similar to that used by Zins et al. Specifically, we have studied several multiply charged cationic species formed upon electrospraying the halide salt of 1,5,15,20-tetrakis(alpha-pyridinio-methylphenyl)-(2H)-porphyrin, "$[H_2P]X_4$", from solution. These species can carry up to four positive charges, dependent on the number of counterions (bromine) present. In further contrast to the substituted benzylpyridinium (mono)cations used previously, they now comprise up to four benzylpyridinium groups attached to a porphyrin ring. As a consequence, we expect to see a fragmentation cascade with up to four pyridine losses, see Scheme 1 (shown for the bromine-free tetracation $[H_2P]^{4+}$).

The purpose of this work is 2-fold: first, we want to explore and possibly expand the validity range of benzylpyridinium-based ions as thermometers for the collision induced dissociation of (multiply charged) gaseous ions in ion-trap instruments, especially in combination with Orbitrap mass analyzers. Second, we want to use the extended thermometer scale to estimate the height of the Coulomb barrier for several multiply charged metalloporphyrin oligomers. The latter application is part of an ongoing project that is focused on the gas-phase structure, energetics, and cooperative bonding interactions of metalloporphyrin oligomer ions [35–38].

Experimental

Sample Preparation

For the preparation of the small benzylpyridinium salts we followed literature procedure. Specifically, the corresponding

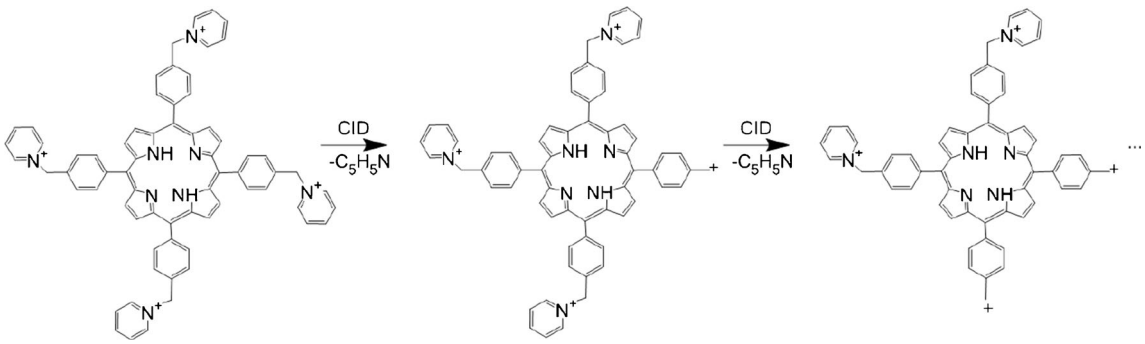

Scheme 1. Fragmentation cascade of 1,5,15,20-tetrakis(alpha-pyridinio-methylphenyl)-(2H)-porphyrin

halides were obtained from Sigma Aldrich and treated with an excess of pyridine at 60 °C for 3 h. After cooling to room temperature, unreacted pyridine is removed by evaporation at reduced pressure. The chloride salts were dissolved in methanol or water and used without further purification. The metal-free pyridinium porphyrin "$[H_2P]B_4$" was synthesized according to literature procedures [39]. The metalation of pyridinium porphyrine is performed as follows: 25 mg (0.025 mmol; 1 eq.) of the pyridiniumporphyrine were dissolved in 3 mL of water and treated with a solution of copper(II)acetate monohydrate (25 mg; 0,125 mmol; 5 eq.) in a minimal amount of water. The reaction mixture was kept in the dark and stirred overnight at room temperature, whereupon the solvent was removed under reduced pressure. The resulting dark residue of metalated porphyrin was washed with a small amount of chloroform and used without further purification.

Instrumental

The experiments were performed with a Thermo LTQ XL Orbitrap mass spectrometer using a standard electrospray ion source. The source conditions were: aqueous solution (0.1 mmol/l) of $[H_2P]Br_4$, flow rate 3 µL/min, spray voltage ca. 3 kV, nitrogen as sheath gas, and transfer capillary heated to 150 °C. The ions emerging from the source are guided by a set of lenses and rf ion guides into a linear rf ion trap filled with ca. $4{\cdot}10^{-3}$mbar of helium. Prior to the CID measurement, the parent ion of interest is isolated by removing all unwanted ions from the trap via the application of an appropriate rf-sweep. For this, the center of the isolation range is set to the first peak of the respective isotope distribution (within 0.01 u). The corresponding isolation width is set to 3 u (unless noted otherwise). Subsequently, the species remaining after isolation are excited by a rf pulse. Unless otherwise noted, we kept the pulse length constant at 30 ms. During this pulse the ions are accelerated by the rf field, excited by collisions with the residual helium gas in the ion trap until they dissociate. The pulse amplitude [in instrument-specific units of "normalized collision energy" (%NCE)] is varied systematically in order to obtain breakdown curves; see below. As a consequence of the resonant rf excitation, all ensuing fragments are off-resonance and are therefore not excited further. The fragments that are observed originate directly from the parent ion, i.e., the fragment distribution exhibits far less secondary fragmentation than in conventional, energy-resolved CID experiments, e.g., using triple quadrupole instruments in which the parent ions are injected into a collision gas cell at high energy. For detection, parent and fragment ions are transferred into the Orbitrap and the fragment mass spectrum is recorded with high mass resolution. This is the main difference to the setup used by Zins et al. [13] in which both excitation and detection were performed in the same linear ion trap.

In the instrument software, the excitation amplitude is given in "NCE units". This is not the actual rf voltage in volts, V. Instead, the relation is $V = NCE \cdot (a \cdot (m/z) + b)$ with a and b instrument-specific (positive) parameters. Therefore, the actual voltage applied for a given NCE value increases linearly with the mass-to-charge ratio of the respective ion. The underlying idea is that regardless of which molecules, the number of vibrational-degrees-of-freedom scales roughly the same way as their molecular mass increases. Under this idealized assumption all chemically related species with the same fragmentation energy but different *m/z* should show the same degree of fragmentation at the same excitation amplitude setting (in units of NCE).

Computational

We performed full geometry optimizations for all parent and fragment ions (see below) using density functional theory with the BP86 functional and def-SVP basis set as implemented in the Turbomole package. The theoretical fragmentation energy is calculated as the difference between the total energy (without zero point energy) of the parent benzylpyridinum ion and the sum of the total energies of the respective benzylium ion and neutral pyridine fragments. We assume that the fragmentation pathway is identical for all losses, with no reverse barrier. However, the benzylium fragment can isomerize into a tropylium ion, which is often slightly lower in energy [13, 40, 41]. On the other hand, the formation of a seven-membered ring requires a substantial bond rearrangement and, consequently, is expected to have a significant (additional) activation barrier. In an IRMPD spectroscopy study it has been shown that such isomerization occurs on longer timescales than relevant for CID studies and can therefore be neglected in corresponding applications of (small, singly charged) benzylpyridinium ions [32]. Compared with the latter and also taking into account their much larger number of degrees of

freedom, we expect that the isomerization of H_2P-based cations to tropylium fragments should be even slower (at similar energies). Nevertheless, we have calculated the total energies of both the benzylium and tropylium fragment ions generated following the first pyridine loss: they are almost isoenergetic, the tropylium being 2 kJ/mol lower (see Figure 5). Specifically, we calculate the fragmentation energies as 221 kJ/mol to generate the benzylium and 219 kJ/mol for the tropylium fragment ion (+ pyridine), i.e., the small energy difference is negligible compared with the much larger fragmentation energy.

Results

Figure 1 shows a typical mass spectrum obtained by electrospray ionization of an aqueous solution of $[H_2P]Br_4$. The spectrum is dominated by quadruply and triply charged species, especially by $[H_2P]^{4+}$ and $[H_2P+Br]^{3+}$. In-source fragmentation, i.e., loss of one or several pyridine units leading to $[H_2P–n\ py\ ]^{4+}$ and $[H_2P+Br-\ n\ py]^{3+}$ is generally observed as well. Its extent depends on the source conditions. In addition to adducts of bromine counterions, some triply charged species also result from deprotonation. Since the masses of bromine and pyridine are close, the isotope distributions of the deprotonated parent ion $[HP]^{3+}$, and the fragment $[H_2P\text{-}py+Br]^{3+}$ overlap (see inset of Figure 1). This is only a minor complication as all peaks can easily be mass-resolved by the Orbitrap used in this study.

In the subsequent CID experiments, each of the species indicated in Figure 1 was isolated and excited by applying the appropriate resonant rf-pulse (as detailed in Experimental). In most cases we observe loss of one neutral pyridine molecule as the dominating fragmentation channel, see Figure 2. However, at the same nominal NCE, the relative fragment intensity strongly depends on the respective parent ion: at 10% NCE, more than 50% of the $[H_2P]^{4+}$ ions are dissociated into $[H_2P\text{-}py]^{4+}$ and pyridine. At the same NCE $[H_2P\text{-}3py]^{4+}$ is quite stable. Its relative fragment ion intensity is smaller than 5% - see Figure 2d. $[H_2P\text{-}py]^{4+}$ and $[H_2P\text{-}2py]^{4+}$ are intermediate, see Figure 2b and c.

Increasing the collision energy to 15% NCE leads to increased fragmentation in all cases. Under these conditions $[H_2P]^{4+}$ is almost completely dissociated, whereas for $[H_2P\text{-}3py]^{4+}$ the dissociation is observed to set in. Again, the other species are intermediate; see Supplementary Figure S2. For $[H_2P]^{4+}$ and $[H_2P\text{-}py]^{4+}$ the only fragmentation channel is loss of one neutral pyridine molecule (Supplementary Figure S2a and b), loss of two pyridines accounts for less than 1% of the total fragment intensity. For $[H_2P\text{-}2py]^{4+}$, pyridine loss is still the dominating fragmentation channel, but loss of CH_3 and of protonated pyridine (leading to a triply charged fragment) are observed as minor channels as well; see Supplementary Figure S2c. For $[H_2P\text{-}3py]^{4+}$ the situation is reversed: CH_3 loss and loss of protonated pyridine dominate over loss of neutral pyridine. This can be understood on the basis of the increasing electron affinity of the $[H_2P\text{-}npy]^{4+}$ species; see Supplementary Figure S1. While the brominated species $[H_2P+Br]^{3+}$, $[H_2P\text{-}py+Br]^{3+}$, $[H_2P\text{-}2py+Br]^{3+}$, and $[H_2P+2Br]^{2+}$ show the typical simple pyridine loss fragmentation pattern as well, this behavior is more difficult to reconcile with expectations from DFT calculations. These indicate that the energetically favored fragmentation product does not in fact correspond to a zwitterion with separate multicationic benzylium group and bromine anion. Instead, in the favored fragment ion structure, the bromine forms a covalent bond with the terminal CH_2-group of the benzylium subunit (see Supplementary Figures S3 and S4). Obviously, accessing such a structure from the parent ion does not involve just simple bond cleavage and pyridine loss, but instead requires significant atom rearrangement. Therefore the process is expected to have an additional activation barrier with an overall height that depends on the relative position of the counterion and leaving pyridine group (see below). There are several possible isomers. It is not clear how large the relative abundances of these different isomers are in our ion-trap. As a consequence, we neglect the bromine-containing species and use only the quadruply charged ions $[H_2P]^{4+}$, $[H_2P\text{-}py]^{4+}$, and $[H_2P\text{-}2py]^{4+}$ as well as the deprotonated triply charged ions $[HP]^{3+}$ and $[HP\text{-}py]^{3+}$ for "thermometer ion" calibration.

The calibration procedure is as follows: for each of these five species, we determine the breakdown curve, i.e., the relative parent intensity (ratio of the parent ion intensity and the total ion intensity) as function of the instrumental excitation energy in units of NCE; see Figure 3[1]. Subsequently, we fit a function of the type $f(E) = A \cdot \left[1 - \frac{1}{1+\exp[B\cdot(E_{50\%}-E)]}\right]$ to the data. Such an exponential fit is the obvious choice to reflect an Arrhenius-like fragmentation activation energy and the systematically varied internal energy distribution of the parent ions [13]. Parameter A takes into account that some of the parent ions might already fragment upon isolation, i.e., even at a nominal excitation energy of zero. It turns out that this is not the case, i.e., parameter A is close to 100% (within 3%). Parameter B describes the steepness of the fit function. The threshold energy, $E_{50\%}$, is defined as the energy at which the relative parent ion intensity is reduced to 50%.

For "thermometer ion" calibration, the $E_{50\%}$ values then need to be correlated with the calculated dissociation energies (as indicated in Table 1 and Supplementary Figure S1). As discussed above, these dissociation energies are obtained as differences of the total energies of the respective parent and fragment ions plus the energy of the outgoing neutral pyridine group, which amounts to –248.106626 in atomic units. All geometries are fully optimized; the structures and

[1]Since the benzylpyridinium porphyrins can lose pyridines via several identical paths (for example four in case of $[H2P]^{4+}$, three in case of $[H_2P\text{-}py]^{4+}$), one might include a multiplicity factor, i.e. calculate the total ion intensity by sum of fragment intensity, divided by this multiplicity factor, and parent intensity. This procedure slightly shifts the breakdown curves to larger values, see Table 1.

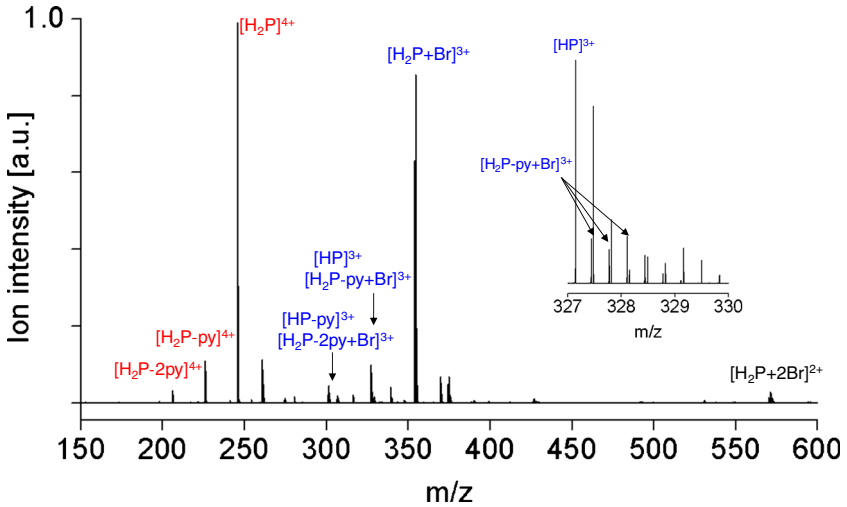

Figure 1. Typical ESI mass spectrum of 1,5,15,20-tetrakis(alpha-pyridinio-methylphenyl)-(2H)-porphyrin tetrabromide "$[H_2PBr_4]$". The black, blue, and red labels refer to doubly, triply, and quadruply charged cations, respectively; "py" stands for pyridine

corresponding total energies are shown in Supplementary Figure S1. As a general rule, the dissociation energy increases with charge state. Furthermore, for the same charge, the dissociation energy increases as the number of pyridine units that remain attached to the respective porphyrinic fragment ion decreases. This reflects the fact that higher charge states are better stabilized by larger and therefore more polarizable ions. Or put another way, the closer the charges, the larger the intramolecular Coulomb repulsion (and the less stable the resulting porphyrinic fragment). See Supplementary Figure S1 for a charge distribution on parent and fragment based on Mulliken-population analysis.

As can be seen in Figure 4, the experimental threshold energies, $E_{50\%}$, and the respective calculated dissociation energies, E_{Diss}, are indeed highly correlated (filled red circles). A linear fit with intercept fixed to zero describes the relation well, i.e., E_{Diss}[kJ/mol] and $E_{50\%}$[%NCE] are proportional to each other with a proportionality factor of 21.2 [kJ/(mol·%NCE)]. Allowing for a variable intercept does not significantly improve the quality of the fit, see Figure 4.

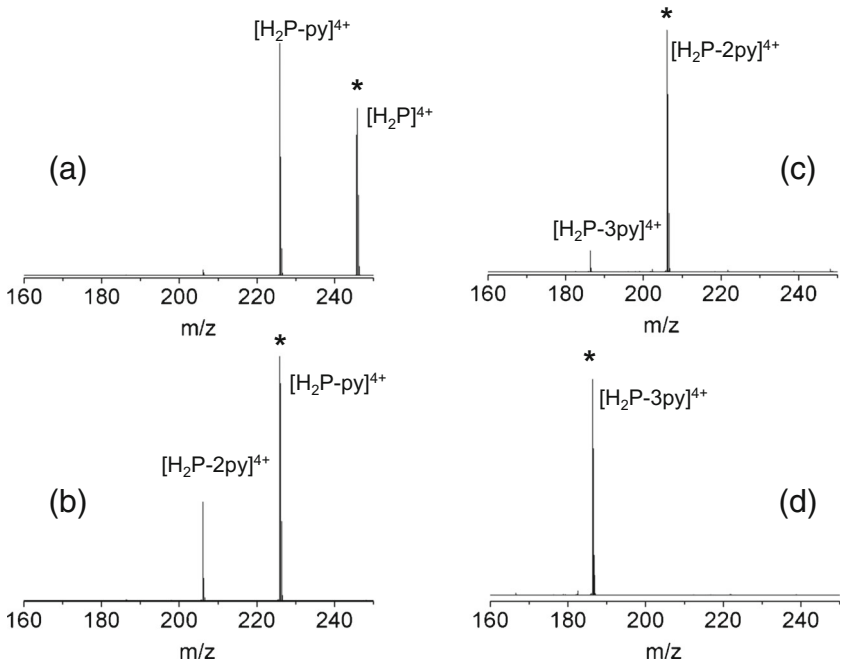

Figure 2. Typical CID measurements for quadruply charged $[H_2P\text{- n py}]^{4+}$ ions, n = 0–3. The respective parent ions (indicated by stars) were isolated in the ion trap and excited by a rf-pulse to probe fragments generated at a fixed excitation energy. The resulting fragment ions were detected in the Orbitrap. All parameters were kept constant except for the parent ion mass (which was set to the first peak of the respective isomer distribution). The isolation width was set to 3 u, the excitation energy (NCE) to 10%, and the pulse duration 30 ms

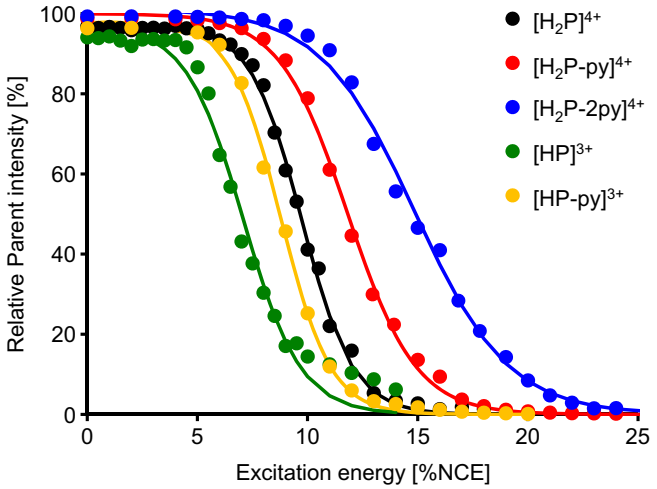

Figure 3. Breakdown curves of the thermometer ions considered, i.e., relative parent intensity [$I_{Parent}/(I_{Parent}+I_{Fragment})$] as a function of the excitation energy ("normalized collision energy", in % NCE) for the quadruply charged $[H_2P\text{- n py}]^{4+}$ ions, n = 0, singly, doubly, and the triply charged ions $[HP\text{- n py}]^{3+}$, n = 0, 1. The lines correspond to an exponential fit to the data; see text. For each fragmentation curve three runs were conducted. The statistical error on each data point is 5%

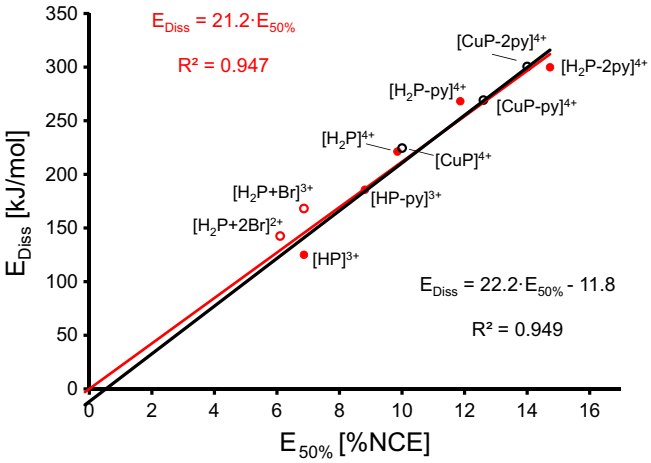

Figure 4. Correlation between experimentally determined fragmentation thresholds ($E_{50\%}$ values) and dissociation energies calculated at the DFT level. The red filled circles are the bromine-free, $[H_2P]$-based porphyrin cations used for calibration. The red open circles correspond to adducts of the latter with bromine counterions. The black open circles represent analogous [CuP]-based porphyrin cations. Only the bromine-free, $[H_2P]$-based porphyrin cations were used for calibration; see text. The black line corresponds to a linear fit optimizing both the slope and the intercept. The red line corresponds to a linear fit with the intercept fixed to zero

As already mentioned above, the triply and doubly charged aggregates of the porphyrin cation with bromine counterions $[H_2P+Br]^{3+}$, $[H_2P\text{-}py+Br]^{3+}$, $[H_2P\text{-}2py+Br]^{3+}$, and $[H_2P+2Br]^{2+}$ show the same simple pyridine loss fragmentation pattern. Based on our DFT-calculations, the resulting zwitterions (i.e., the isomers in which the bromine anion is bound ionically rather than covalently to the porphyrin fragment ion) do not represent the lowest energy form of the respective fragments (see Supplementary Figures S3 and S4). The zwitterionic isomer is 153 kJ/mol less stable than the $[H_2P\text{-}py+Br]^{3+}$ isomer in which the bromine is covalently bound to the terminal benzylic CH_2 moiety resulting from pyridine loss. In the former case, the fragmentation energy (calculated as the difference of ground state energies of parent and fragment ions) is 168 kJ/mol, in the latter case it is only 15 kJ/mol. However, the energy required to reach the zwitterionic isomer represents a plausible approximation to the kinetically limiting dissociation barrier because one can expect that the intramolecular neutralization by addition of the bromine anion to the cationic CH_2 group would occur only *after* the pyridine dissociation step. If this is true, $[H_2P+Br]^{3+}$ should show a similarly good correlation with the experimental thresholds as is the case for the five bromine-free species discussed above. This is indeed the case: for $[H_2P+Br]^{3+}$ we measure a threshold energy, $E_{50\%}$, of 6.9. If we multiply this with the proportionality factor of 21.2 obtained from our previous calibration procedure, we get 146 kJ/mol, in reasonable agreement with the value of 168 kJ/mol calculated for dissociation into the zwitterionic structure. For the doubly charged $[H_2P+2Br]^{2+}$ the situation is similar. For dissociation into pyridine and the zwitterionic porphyrin fragment we calculate a total energy difference of 143 kJ/mol. With the covalently bound fragmentation product we calculate only a difference of 6 kJ/mol. Experimentally, we obtain a $E_{50\%}$ value of 6.1, which translates into an energy barrier of 129 kJ/mol, again in reasonable agreement with the energy difference obtained by DFT for the zwitterionic fragment. Both data points are included in Figure 4 as red open circles (but not used in the calibration fit). We did not perform a similar comparison of the fragmentation thresholds of $[H_2P\text{-}py+Br]^{3+}$ ($E_{50\%}$: 7.9) and $[H_2P\text{-}2py+Br]^{3+}$ ($E_{50\%}$: 13.2) with corresponding DFT calculations, since it is not clear whether the two parent ions are zwitterionic or not (note that these species result from in-source fragmentation of $[H_2P+Br]^{3+}$

Table 1. Experimentally Determined Normalized Collision Energies (NCE) Required to Achieve Equal Parent and Fragment Ion Intensities, $E_{50\%}$ (Given in %NCE), for Five Multiply Charged Benzylpyridinium-Porphyrin Ions. These are Contrasted to Quantum Chemically Calculated Dissociation Energies for the Same Process

	$E_{50\%}$ [% NCE][b] exptl.	E_{Diss} (kJ/mol) calc.
$[H_2P]^{4+} \rightarrow [H_2P\text{-}py]^{4+} + py$	9.7 ± 0.2	221
$[H_2P\text{-}py]^{4+} \rightarrow [H_2P\text{-}2py]^{4+} + py$	11.9 ± 0.2	268[a]
$[H_2P\text{-}2py]^{4+} \rightarrow [H_2P\text{-}3py]^{4+} + py$	14.7 ± 0.2	300[a]
$[HP]^{3+} \rightarrow [HP\text{-}py]^{3+} + py$	6.9 ± 0.2	125
$[HP\text{-}py]^{3+} \rightarrow [HP\text{-}2py]^{3+} + py$	8.8 ± 0.2	186

[a]Note that for $[H_2P\text{-}2py]^{4+}$ both cis and trans isomers were considered (see Figure 6); they differ in energy by 0.6 kJ/mol, which is negligible.
[b]Introduction of path multiplicity factors shifts the breakdown curves and consequently $E_{50\%}$ to slightly larger values; for $[H_2P]^{4+}$ we obtain 11.4 [%NCE], for $[H_2P\text{-}py]^{4+}$ 13.6, for $[H_2P\text{-}2py]^{4+}$ 15.6, for $[HP]^{3+}$ 9.6, and for $[HP\text{-}py]^{3+}$ 10.0.

followed by transfer into the ion trap, i.e., there is ample time available for rearrangement). The same holds true for their fragments $[H_2P\text{-}2py+Br]^{3+}$ and $[H_2P\text{-}3py+Br]^{3+}$.

Robustness of Calibration

Before using such a thermometer ion calibration to analyze the fragmentation of related systems, it is important to consider the reproducibility of breakdown curves and related threshold energies, $E_{50\%}$. The mass spectra, i.e., the relative intensities of doubly, triply, and quadruply charged ions, as well as the relative amounts of pyridine loss fragments, depend strongly on ion source conditions such as spray voltage, capillary temperature, and tube lens voltage. In contrast, within the error limits of the experiments (±0.2 NCE, see Table 1), the breakdown curves and resulting $E_{50\%}$ values *do not* depend on source conditions. This implies that the parent ions are sufficiently thermalized after transfer and storage in the ion trap, prior to the rf-activation step. Not surprisingly, there is a pronounced dependence of breakdown curves on the exact position of the excitation window – relative to the isotopomer distribution of the ions to be excited. We therefore consistently set the excitation position exactly (to within 0.01 mass units) on top of the first peak in the isotope distribution of the respective parent ion. Additionally, the breakdown curves depend strongly on the excitation time. Supplementary Figure S5a shows measurements for excitation times of 30, 100, and 300 ms, respectively. These indicate that a 10-fold increase in excitation time decreases $E_{50\%}$ values roughly by 20%. For all measurements, the excitation time was therefore kept constant at 30 ms. The breakdown curves depend slightly on the isolation width (see Supplementary Figure S5b) as well. This reflects the fact that the parent ions may already be excited by the isolation procedure. A small isolation window requires a rf-sweep with frequencies close to the resonance frequency of the respective parent ion. Therefore we kept the isolation width constant at 3 u for all measurements. Under these conditions (and if all of the other ion trap potentials and the activation time are kept constant), the determination of $E_{50\%}$ is highly reproducible, see Supplementary Figure S5c. For each data point the ion signal was integrated for 1 min, i.e., the determination of each breakdown curve took less than 30 min and the entire calibration procedure could be performed within 2 hours.

Test Case: Metalloporphyrins

Next we checked the calibration using a closely related test case: 1,5,15,20-Tetrakis(alpha-pyridinio-methylphenyl)-(Cu)-porphyrin "CuP", which differs from the free-base "H_2P" thermometer ion system only by substitution of two central protons by one Cu^{2+}. The mass spectrum and fragmentation pattern closely resemble that of the free-base congener "H_2P". Pyridine loss is the dominant fragmentation channel and again we expect no reverse barrier. The experimentally determined fragmentation threshold energies should therefore again correlate to the thermodynamic dissociation energies. Based on the respective breakdown curves (not shown), we obtain $E_{50\%}$ values of 10.0 for $[CuP]^{4+}$, 12.6 for $[CuP\text{-}py]^{4+}$, and 14.0 for $[CuP\text{-}2py]^{4+}$, respectively. Using the calibration constant of 21.2 (see above), this translates to fragmentation energies of 212, 272, and 297 kJ/mol, respectively. On average, these values deviate by less than 5% from the DFT-calculated dissociation energies, see Table 2 and Figure 4. As before, the parent and fragment geometries are fully optimized. The close relationship between experimental and calculated energies implies that this method can be used as a tool to estimate fragmentation barriers – at least for similar (porphyrin) systems.

Comparison with Small Benzylpyridine Cations

In order to test the limits of the benzylpyridine-porphyrin-ion based energy calibration (Table 1), we next measured a set of 10 small, singly charged benzylpyridinium-cations (Table 3) – a data set similar to the one used by Zins et al. [13]. We used the same ion trap parameters (width 3 u, 30 ms excitation time) as before, and detected both parent and fragment ions in the Orbitrap. In all cases, we observed loss of pyridine as the only fragmentation channel. We obtain similar, highly reproducible breakdown curves that allow us to determine $E_{50\%}$ with an accuracy of ±0.1 NCE. The thermodynamic dissociation energies of the small benzylpyridinium ions were obtained by DFT calculations with the same functional and basis set as for the benzyl-pyridine-porphyrin multications. As before, we observe a linear relation between the experimental $E_{50\%}$ values and the quantum chemically obtained dissociation energies. However, as can be seen from Figure 5a, the slope of the line for small, singly charged benzylpyridinium-cations differs completely (by more than a factor of five) from that obtained for the multiply charged benzylpyridinium-porphyrin cations – even though the dominant fragmentation channel is the same in both cases. A possible reason is that the ion transfer to the Orbitrap (after CID in the ion trap) depends on the mass-to-charge ratio and/or mobility of parents and fragments. For the benzyl-pyridine-porphyrins both parent and fragment ions have similar masses (within 10%) while for the small thermometer ions the fragments have only 50%–67% of the parent mass. As a consequence, we reanalyzed the data by calculating the relative parent ion intensity (normalized against parent ion intensity at NCE = 0) as a function of NCE. This method has the advantage that it is not prone to mass-dependent ion transfer since it focuses only on the parent mass; the disadvantage is that it is

Table 2. $E_{50\%}$ Values (Given in %NCE) for Three Quadruply Charged Copper-Benzylpyridinium-Porphyrin Ions. These are Compared to Quantum Chemically Calculated Dissociation Energies

	$E_{50\%}$ [% NCE] exp.	E_{Diss} (kJ/mol) exp.	E_{Diss} (kJ/mol) calc.
$[CuP]^{4+} \rightarrow [CuP\text{-}py]^{4+} + py$	10.0 ± 0.2	212	225
$[CuP\text{-}py]^{4+} \rightarrow [CuP\text{-}2py]^{4+} + py$	12.6 ± 0.2	272	269
$[CuP\text{-}2py]^{4+} \rightarrow [CuP\text{-}3py]^{4+} + py$	14.0 ± 0.2	297	301

Table 3. $E_{50\%}$ (Given in %NCE) Values and Quantum Chemically Calculated Dissociation Energies for Small Substituted Benzylpyridinium Ions

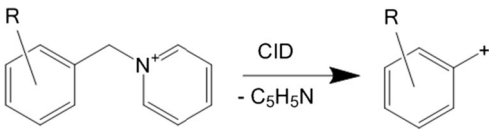

Substitution	$E_{50\%}$ [% NCE] exp.	E_{Diss} [kJ/mol] calc.
m-CH_3	35.3 ± 0.1	233
o-CH_3	34.1 ± 0.1	226
p-CH_3	33.6 ± 0.1	218
p-OCH_3	23.3 ± 0.1	179
p-F	34.8 ± 0.1	228
p-Cl	31.7 ± 0.1	224
p-CN	38.4 ± 0.1	258
p-CF_3	36.9 ± 0.1	257
p-tert-Butyl	24.9 ± 0.1	205
Pentamethyl	16.7 ± 0.1	172
2,4-Dimethyl	27.9 ± 0.1	201

much more sensitive to ESI source intensity fluctuations. As can be seen in Supplementary Figure S6, this procedure somewhat improves the individual fits, but does not solve the fundamental problem, namely that the two thermometer scales are incompatible. Another possible reason is that the NCE scale might not correctly take the charge into account: as it is implemented in the instrument software, the rf excitation voltage applied is a linear function of the mass-to-charge-ratio only (see Introductory part). The charge alone is not a parameter that can be set (only NCE, *m/z*, isolation width, and excitation time). The idea behind this is that for two ions with the same mass-to-charge ratio, the one with the higher charge consequently has a larger number of atoms (assuming similar composition) and therefore more vibrational degrees of freedom. As a consequence, its kinetic shift is larger, i.e., for a given internal energy the fragmentation is slower. However, due to the higher charge, the ion gains a higher internal energy and ideally this cancels the larger kinetic shift so that for a given time window the fragmentation ratios of all ions with same *m/z* should be equal. Obviously, as can be seen in Figure 5a, this is not true. As a consequence, we multiplied the $E_{50\%}$-values by the charge, i.e., by 4 for [H2P-n py]$^{4+}$. As can be seen in Figure 5b, this ad hoc procedure works reasonably well, and both small and large thermometer ions almost fall on a single line. Apparently, for a charge-independent calibration, the NCE scale has to be multiplied by the charge of the respective ion.

In order to validate our conclusions, we repeated the CID experiments on another instrument (Waters Synapt G2). Here the ions are accelerated by a traveling voltage wave through a gas (Ar) filled collision cell. The resulting fragment ions are guided through the ion mobility cell and are analyzed by a reflectron time-of-flight mass spectrometer. By variation of the acceleration voltage and integration the parent and fragment ion intensities we obtain similar breakdown curves as for the LTQ orbitrap instrument. As before, the calibration curves for both small and large thermometer ions are internally consistent, but both calibration curves differ significantly as well. In this case both curves cannot be reconciled by multiplication with the charge (see Supplementary Figure S11a and b).

Estimation of Fragmentation Barriers for Porphyrin Dimers

We next apply our benzylpyridine-porphyrin based energy calibration to examine the fragmentation energies of larger oligomers of multiply negatively charged substituted metalloporphyrins such as tetra(4-sulfonatophenyl)porphyrins

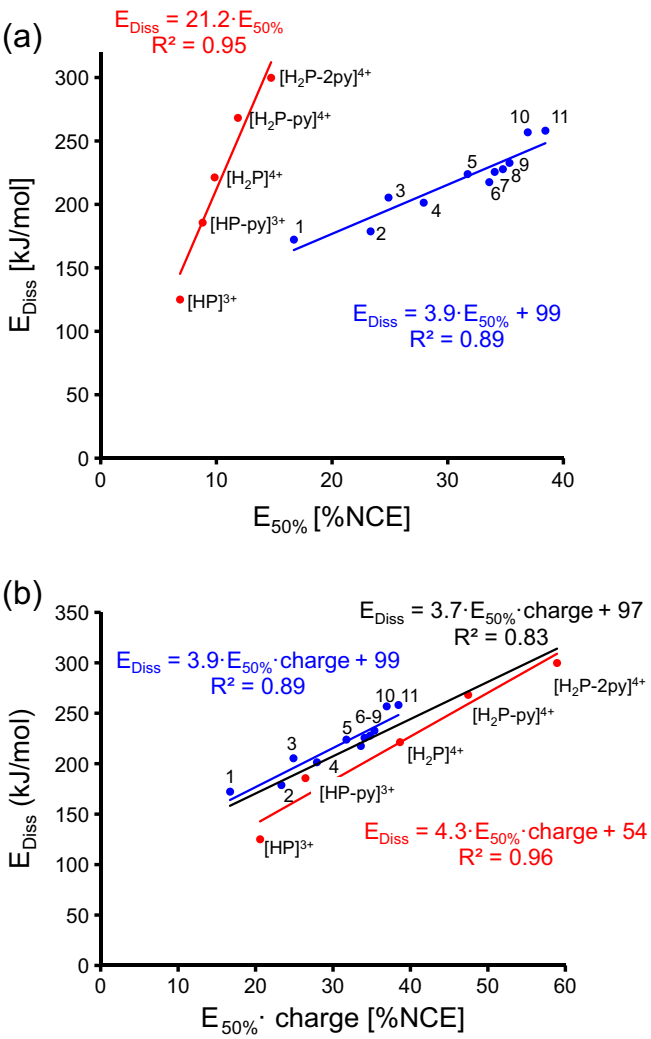

Figure 5. Comparison of the calibration curves obtained for multiply charged [H_2P]-based cations (red dots), small singly charged benzylpyridinium ions (blue dots). The numbers correspond to the different substitutions: 1 = pentamethyl, 2 = p-OCH_3, 3 = p-tert-butyl, 4 = 2,4-dimethyl, 5 = p-Cl, 6 = p-CH_3, 7 = o-CH_3, 8 = p-F, 9 = m-CH_3, 10 = p-CF_3, 11 = p-CN; see text. **(a)** The $E_{50\%}$ of the respective ions are unscaled, i.e., as obtained from the breakdown curves, **(b)** the $E_{50\%}$ are multiplied by the charge of the respective ions, i.e., multiplied by 4 for [H_2P-n py]$^{4+}$ and 3 for [HP-n py]$^{3+}$

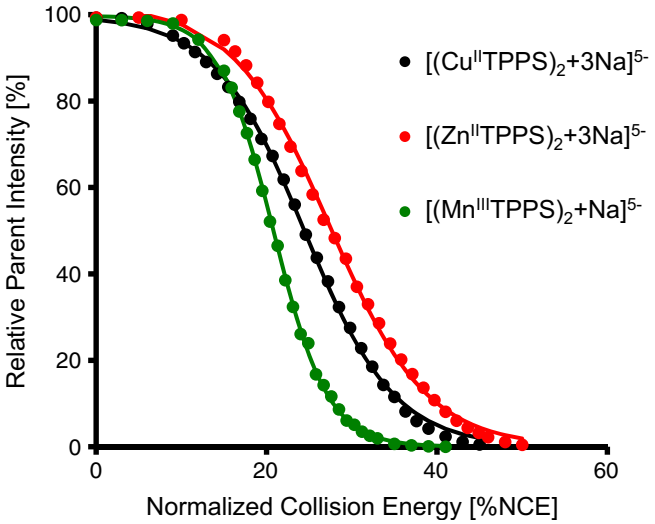

Figure 6. Breakdown curves for different porphyrin dimer multi-anions. Relative parent intensity as function of normalized collision energy for $[(Mn^{III}TPPS)_2+Na]^{5-}$, $[(Cu^{II}TPPPS)_2+3Na]^{5-}$, and $[(Zn^{II}TPPPS)_2+3Na]^{5-}$. Since the Orbitrap is a charge-sensitive detector, we have to correct the ion intensity for the charge (i.e., divide each ion intensity by the respective charge), and since each parent ion gives rise to two fragment ions, we average the intensities of the fragments; i.e., the relative parent intensity is calculated as: $I_{p,r} = \frac{I_p/5}{I_p/5+\frac{1}{2}(I_{f1}/3+I_{f2}/2)}$. For each fragmentation curve two runs were conducted. The statistical error on each data point is 5%

(TPPS) with different metal centers (Zn^{II}, Cu^{II}, and Mn^{III}). From previous studies we know that MTPPS species easily oligomerize in gas phase [35, 36, 38]. Supplementary Figure S7a shows a typical ESI mass spectrum of a 1 mmol/l aqueous solution of Mn^{III}TPPS. Besides the dominating monomers in the –3 charge state (which have several different comparable-in-magnitude collision induced decay channels and were therefore not studied), dimers in different charge states account for ca. 10% of the total ion intensity. For the dimer in charge state –5, the dominant fragmentation channel is dissociation into the corresponding doubly and triply charged monomers, see Supplementary Figure S7b. This means that the dimer fragmentation pattern is almost as simple as that for the thermometer ions used for calibration, i.e., in both cases only one fragmentation channel has to be taken into account and the fragmentation is basically the cleaving of one bond, i.e., there is no significant structural rearrangement of the fragments after dissociation. The main difference is that now both fragments are charged, which leads to an electrostatic Coulomb barrier. This can easily be understood by looking at the reverse process: at large distances two well separated, charged fragments (of the same polarity) can be approximated as point charges. They are then subjected to a Coulomb repulsion that is inversely proportional to their separation. When this distance is reduced, the charged fragments have to pass over a repulsive Coulomb barrier before they can associate and form a (covalent or ionic) bond. This barrier strongly depends on the electronic properties of the corresponding ions, such as their charge distribution and polarizability. It can easily range up to several electron volts in height.

In a previous publication, we had determined the breakdown curves of $[(Mn^{III}TPPS)_2+H]^{5-}$ [35]. Note that these curves are not comparable with the present energy calibrations since the excitation parameters differed in the former study. Now, using the same parameters as for the "H_2P" calibration, we obtain the breakdown curves as shown in Figure 6. The derived threshold energies $E_{50\%}$ are 20.7 [%NCE] for $[(MnTPPS)_2+Na]^{5-}$ (Figure 6). For the analogous protonated species, we obtain similar values, 20.8, reflecting the fact that for TPPS-dimers with trivalent metal centers, the counterions are not involved in the bond between the monomeric subunits [35]. Using the linear calibration function obtained for all benzylpyridine thermometer ions ($E_{Diss} = 3.7\ E_{50\%}$·charge+97, see Figure 5b, black line) this translates into a fragmentation activation energies of 480 kJ/mol. (Ignoring the charge, i.e., using the scaling factor of 21.2, cf. Figure 5a, we obtain 440 kJ/mol; see Table 4).

For $[(Cu^{II}TPPS)+3Na]^{5-}$ and $[(Zn^{II}TPPS)+3Na]^{5-}$ we obtain threshold energies, $E_{50\%}$, of 24.5 [%NCE] and 27.4 [%NCE], which translates to 550 kJ/mol and 600 kJ/mol, respectively, with the linear calibration ($E_{Diss} = 3.7\ E_{50\%}$·charge + 97). Both values are similar, reflecting the fact that the TPPS-dimers with a divalent metal center are bound by ionic interactions between the sodium counterions and the sulfonic acid groups and the transition metal centers are not directly involved in the cohesion [38]. For the closed-shell (d^{10}) ZnTPPS we performed DFT calculations (BP-86, def-SVP basis set) and obtained 120 kJ/mol for the fragmentation of the Zn-dimer according to the scheme $[(Zn^{II}TPPS)+3Na]^{5-} \rightarrow [(Zn^{II}TPPS)+Na]^{3-} + [(Zn^{II}TPPS)+2Na]^{2-}$ (not zero-point-energy corrected energy difference of the optimized parent and fragment structures). The experimental threshold energy of 600 kJ/mol is significantly larger than this energy difference of 120 kJ/mol. Note that our experiment indicates the presence of a substantial Coulomb barrier to fragmentation. We have explored the corresponding multidimensional Coulomb barrier surface of $[(Zn^{II}TPPS)+3Na]^{5-}$ theoretically by performing model calculations at the DFT-level (BP-86, def-svp), see Supplementary Figure S8. The barrier height obtained (625 kJ/mol) in this calculation is in reasonable agreement (within 5%) with the experimental threshold energy (600 kJ/mol) as calibrated with the thermometer ion based scale,

Table 4. $E_{50\%}$ Values for Various Metalloporphyrin Dimers

	$E_{50\%}$ [% NCE]	$E_{Diss} = 3.7 \cdot E_{50\%}$· charge + 97	$E_{Diss} = 21.2 \cdot E_{50\%}$
$[(Mn^{III}TPPS)_2+H]^{5-}$	20.8 ± 0.5	480 kJ/mol	440 kJ/mol
$[(Mn^{III}TPPS)_2+Na]^{5-}$	20.7 ± 0.5	480 kJ/mol	440 kJ/mol
$[(Cu^{II}TPPS)_2+3Na]^{5-}$	24.5 ± 0.5	550 kJ/mol	520 kJ/mol
$[(Zn^{II}TPPS)_2+3Na]^{5-}$	27.4 ± 0.5	600 kJ/mol	580 kJmol

suggesting that the method remains applicable for metalloporphyrin dimers.

Conclusions

We have explored the suitability range of benzylpyridinium-based "thermometer ions" by performing a collision induced dissociation (CID) and quantum chemical study of various multiply charged (up to +4) cations resulting from electrospray ionization (ESI) of 1,5,15,20-tetrakis(alpha-pyridinio-methylphenyl)-(2H)-porphyrin, "H_2P". As expected for substituted benzylpyridines, a dominant simple fragmentation reaction is observed: loss of neutral pyridine. In addition, H_2P has the advantage that it contains four benzylpyridine units. Thus ESI gives rise to a fragmentation cascade, which provides several fragment species suitable for calibration of the CID-energy scale ("Normalized Collision Energy") via further fragmentation in the linear ion trap of an LTQ-XL Orbitrap mass spectrometer. With five different "H_2P"-derived ions as calibrants, we find the experimentally observed threshold energies, $E_{50\%}$, to be proportional to the quantum chemically calculated dissociation energies to a high degree of accuracy. However, comparing this correlation with analogous measurements of a range of small, singly charged substituted benzylpyridines previously used for calibration, we find large deviations. Multiplying the $E_{50\%}$ values with the respective charge gives a reasonable overall fit for both small, singly charged, and large, triply and quadruply charged thermometer ions. As an application and test, we have also studied multiply negatively charged metalloporphyrin dimers and have applied our thermometer ion- based calibration to gauge the Coulomb barriers for their fragmentation.

Acknowledgments

The authors thank the Deutsche Forschungsgemeinschaft (DFG) for support of this work through the collaborative research center SFB/TRR 88 "3MET" [Kooperative Effekte in homo- und heterometallischen Komplexen; Teilprojekte B2 und C6]. Funding of an Orbitrap mass spectrometer by DFG and Land/KIT (Art 91b) is also gratefully acknowledged.

References

1. Smith, R.D., Barinaga, C.J., Udseth, H.R.: Tandem mass-spectrometry of highly charged cytochrome *c* molecular-ions produced by electrospray ionization. J. Phys. Chem. **93**, 5019–5022 (1989)
2. Armentrout, P.B.: Thermochemical measurements by guided ion beam mass spectrometry. In: Adams, N.G., Babcock, L.M. (eds.) Advances in gas-phase ion chemistry, vol. 1, pp. 83–119. JAI Press, Greenwich (1992)
3. Armentrout, P.B., Ervin, K.M., Rodgers, M.T.: Statistical rate theory and kinetic energy-resolved ion chemistry: theory and applications. J. Phys. Chem. A. **112**, 10071–10085 (2008)
4. Gronert, S.: Quadrupole ion trap studies of fundamental organic reactions. Mass Spectrom. Rev. **24**, 100–120 (2005)
5. Chupka, W.A.: Effect of unimolecular decay kinetics on the interpretation of appearance potentials. J. Chem. Phys. **30**, 191–211 (1959)
6. Sztáray, J., Memboeuf, A., Drahos, L., Vékey, K.: Leucine enkephalin – a mass spectrometry standard. Mass Spectrom. Rev. **30**, 298–320 (2011)
7. Alexander, A.J., Boyd, R.K.: Experimental investigations of factors controlling the collision-induced dissociation spectra of peptide ions in a tandem hybrid mass spectrometer. I. Leucine enkephalin. Int J. Mass Spectrom. Ion Processes. **90**, 211–240 (1989)
8. Schnier, P.D., Jurchen, J.C., Williams, E.R.: The effective temperature of peptide ions dissociated by sustained off-resonance irradiation collisional activation in Fourier transform mass spectrometry. J. Phys. Chem. B. **103**, 737–745 (1999)
9. Wysocki, V.H., Kentamaa, H.I., Cooks, R.G.: Internal energy-distributions of isolated ions after activation by various methods. Int. J. Mass Spectrom. Ion Process. **75**, 181–208 (1987)
10. Voyksner, R.D., Pack, T.: Investigation of collisional-activation decomposition process and spectra in the transport region of an electrospray single-quadrupole mass spectrometer. Rapid Commun. Mass Spectrom. **5**, 263–268 (1991)
11. Kenttamaa, H.I., Cooks, R.G.: Internal energy-distributions acquired through collisional activation at low and high-energies. Int. J. Mass Spectrom. Ion Process. **64**, 79–83 (1985)
12. Derwa, F., de Pauw, E., Natalis, P.: New basis for a method for the estimation of secondary ion internal energy distribution in "soft" ionization techniques. Org. Mass Spectrom. **26**, 117 (1991)
13. Zins, E.-L., Pepe, C., Schröder, D.: Energy-Dependend dissociation of benzylpyridinium ions in an ion-trap mass spectrometer. J. Mass Spectrom. **45**, 1253 (2010)
14. Greisch, J.F., Gabelica, V., Remacle, F., de Pauw, E.: Thermometer ions for matrix-enhanced laser desorption/ionization internal energy calibration. Rapid Commun. Mass Spectrom. **17**, 1847 (2003)
15. Luo, G.H., Marginean, I., Vertes, A.: Internal energy of ions generated by matrix-assisted laser desorption/ionization. Anal. Chem. **74**, 6185 (2002)
16. Collette, C., de Pauw, E.: Calibration of the internal energy distribution of ions produced by electrospray. Rapid Commun. Mass Spectrom. **12**, 165 (1998)
17. Gabelica, V., Schulz, E., Karas, M.: Internal energy build-up in matrix assisted laser desorption/ionization. J. Mass Spectrom. **39**, 579 (2004)
18. Gabelica, V., de Pauw, E.: Internal energy and fragmentation of ions produced in electrospray sources. Mass Spectrom. Rev. **24**, 566 (2005)
19. Naban-Maillet, J., Lesage, D., Bossee, A., Gimbert, Y., Sztaray, J., Vekey, K., Tabet, J.C.: Internal energy distribution in electrospray ionization. J. Mass Spectrom. **40**, 1 (2005)
20. Luo, G.H., Chen, Y., Siuzdak, G., Vertes, A.: Surface modification and laser pulse length effects on internal energy transfer in DIOS. J. Phys. Chem. B. **109**, 24450 (2005)
21. Luo, G.H., Chen, Y., Daniels, H., Dubrow, R., Vertes, A.: Internal energy transfer in laser desorption/ionization from silicon nanowires. J. Phys. Chem. B. **110**, 13381 (2006)
22. Schulz, E., Karas, M., Rosu, F., Gabelica, V.: Influence of the matrix on analyte fragmentation in atmospheric pressure MALDI. J. Am. Soc. Mass Spectrom. **17**, 1005 (2006)
23. Luxembourg, S.L., Heeren, R.M.A.: Fragmentation at and above surfaces in SIMS: effects of biomolecular yield enhancing surface modifications. Int. J. Mass Spectrom. **253**, 181 (2006)
24. Touboul, D., Jecklin, M.C., Zenobi, R.: Ion internal energy distributions validate the charge residue model for small molecule ion formation by spray methods. Rapid Commun. Mass Spectrom. **22**, 1062 (2008)
25. Nefliu, M., Smith, J.N., Venter, A., Cooks, R.G.: Internal energy distributions in desorption electrospray ionization (DESI). J. Am. Soc. Mass Spectrom. **19**, 420 (2008)
26. Pak, A., Lesage, D., Gimbert, Y., Vekey, K., Tabet, J.C.: Internal energy distribution of peptides in electrospray ionization: ESI and collision induced dissociation spectra calculation. J. Mass Spectrom. **43**, 447 (2008)
27. Dagan, S., Hua, Y.M., Boday, D.J., Somogyi, A., Wysocki, R.J., Wysocki, V.H.: Internal energy deposition with silicon nano particle assisted laser desorption/ionization (SPALDI) mass spectrometry. Int. J. Mass Spectrom. **283**, 200 (2009)
28. Tang, H.W., Ng, K.M., Lu, W., Che, C.M.: Ion desorption efficiency and internal energy transfer in carbon-based surface-assisted laser desorption/ionization mass spectrometry: desorption mechanism(s) and the design of SALDI substrates. Anal. Chem. **81**, 4720 (2009)
29. Lecchi, P., Zhao, J.H., Wiggins, W.S., Chen, T.H., Yip, P.F., Mansfield, B.S., Peltier, J.M.: A method for monitoring and controlling reproducibility of intensity data in complex electrospray mass spectra: a thermometer ion-based strategy. J. Am. Soc. Mass Spectrom. **20**, 398 (2009)

30. Barylyuk, K.V., Chingin, K., Balabin, R.M., Zenobi, R.: Fragmentation of benzylpyridinium "thermometer" ions and its effect on the accuracy of internal energy calibration. J. Am. Soc. Mass Spectrom. **21**, 172 (2010)
31. Harris, G.A., Hostetler, D.M., Hampton, C.Y., Fernandez, F.M.: Comparison of the internal energy deposition of direct analysis in real time and electrospray ionization time-of-flight mass spectrometry. J. Am. Soc. Mass Spectrom. **21**, 855 (2010)
32. Morsa, D., Gabelica, V., Rosu, F., Oomens, J., de Pauw, E.: Dissociation pathways of benzylpyridinium "thermometer" ions depend on the activation regime: an IRMPD spectroscopy study. J. Phys. Chem. Lett. **5**, 3787–3791 (2014)
33. Normalized collision energy^{TM} technology. Finnigan (ThermoFisher Scientific) Product Support Bull. 104
34. Steinfeld, J.I., Francisco, J.S., Hase, W.L.: Chemical Kinetics and Dynamics, Prentice Hall, Englewood Cliffs, New Jersey (1989)
35. Schwarz, U., Vonderach, M., Kappes, M., Kelting, R., Brendle, K., Weis, P.: Structural characterization of metalloporphyrin-oligomer multianions by mass spectrometry and ion mobility spectrometry – observation of metastable species. Int. J. Mass Spectrom. **339/340**, 24–33 (2013)
36. Schwarz, U., Vonderach, M., Armbruster, M.K., Fink, K., Kappes, M.M., Weis, P.: Cu(II)- and Mn(III)-porphyrin-derived oligomeric multi-anions: structures and photoelectron spectra. J. Phys. Chem. A. **118**, 369–379 (2014)
37. Weis, P., Schwarz, U., Hennrich, F., Wagner, D., Bräse, S., Kappes, M.M.: Azaporphine guest–host complexes in solution and gas-phase: evidence for partially filled nanoprisms and exchange reactions. Phys. Chem., Chem. Phys. **16**, 6225–6232 (2014)
38. Brendle, K., Schwarz, U., Jäger, P., Weis, P., Kappes, M.M.: Structures of metalloporphyrin−oligomer multi-anions: cofacial versus coplanar motifs as resolved by ion mobility spectrometry. J. Phys. Chem. A. **120**, 8716–8724 (2016)
39. Kubát, P., Lang, K., Anzenbacher Jr., P., Jursíkovád, K., Králd, V., Ehrenberg, B.: Interaction of novel cationic meso-tetraphenylporphyrins in the ground and excited states with DNA and nucleotides. J. Chem. Soc. Perkin Trans. **1**, 933–941 (2000)
40. Zins, E.L., Rondeau, D., Karoyan, P., Fosse, C., Rochut, S., Pepe, C.: Investigations of the fragmentation pathways of benzylpyridinium ions under ESI/MS conditions. J. Mass Spectrom. **44**, 1668 (2009)
41. Zins, E.L., Pepe, C., Rondeau, D., Rochut, S., Galland, N., Tabet, J.C.: Theoretical and experimental study of tropylium formation from substituted benzylpyridinium species. J. Mass Spectrom. **44**, 12 (2009)